

Adaptive Signal Resuscitation: Channel-wise Post-Pruning Repair for Sparse Vision Networks

Qishi Zhan^{1,*,\dagger} Ziheng Chen^{2,*,\dagger} Minxuan Hu³

¹Department of Mathematical and Statistical Sciences, Marquette University, USA

²The University of Texas at Austin, USA

³Cornell Ann S. Bowers College of Computing and Information Science, Cornell University, USA

stokes615@utexas.edu qishi.zhan@marquette.edu

*Equal contribution.

^{\dagger}Corresponding authors, in order: Ziheng Chen and Qishi Zhan.

Abstract

One-shot magnitude pruning can cause severe accuracy collapse in the high-sparsity regime, even when the pruning mask preserves the largest weights. We argue that this failure is driven primarily by a granularity mismatch in post-pruning repair, rather than by the reduction in parameter count alone. Under global magnitude pruning, damage is highly heterogeneous across channels within the same layer: nearly collapsed channels can coexist with channels that retain informative activation variance. Existing layer-wise activation repair methods apply a single correction to the whole layer, and can therefore over-amplify damaged channels while trying to restore the layer-level signal. We propose Adaptive Signal Resuscitation (ASR), a training-free channel-wise repair method that matches the granularity of repair to the granularity of damage. ASR estimates a variance-matching correction for each output channel and stabilizes it with a data-driven shrinkage rule, suppressing unreliable corrections for channels with weak post-pruning signal while preserving corrections for healthier channels. Applied before BatchNorm recalibration, ASR requires only forward passes on a small calibration set and no retraining. Across three datasets, four convolutional architectures, and both unstructured and structured sparsity settings, ASR generally improves over layer-wise repair, with the clearest gains in high-sparsity regimes where repair is most needed. On ResNet-50 at 90% sparsity, ASR recovers 55.6% top-1 accuracy on CIFAR-10, compared with 41.0% for layer-wise repair and 28.0% for BatchNorm-only recalibration. The gains are largest when pruning induces severe and heterogeneous channel damage; in architectures without residual connections, BatchNorm recalibration alone can remain competitive at extreme sparsity. Ablations show that naive channel-wise variance matching is insufficient, and that shrinkage is the key component that stabilizes post-pruning repair.

1 Introduction

Unstructured magnitude pruning remains one of the most practical ways to compress vision networks after training, especially when a trained dense model must be deployed under strict memory or compute constraints [3, 1, 9, 8, 31, 45, 7]. A sparse model can be obtained directly from a trained network without changing the architecture or paying the cost of full retraining. Yet at extreme sparsity, when 90% or more of weights are removed, one-shot magnitude pruning can drive accuracy close to random chance, even when the surviving weights are those ranked most important by the pruning rule [5, 31, 39].

This drop in performance is not explained solely by the removal of important parameters. Global L1 pruning removes weights by magnitude across the entire network, without respect to layer or channel

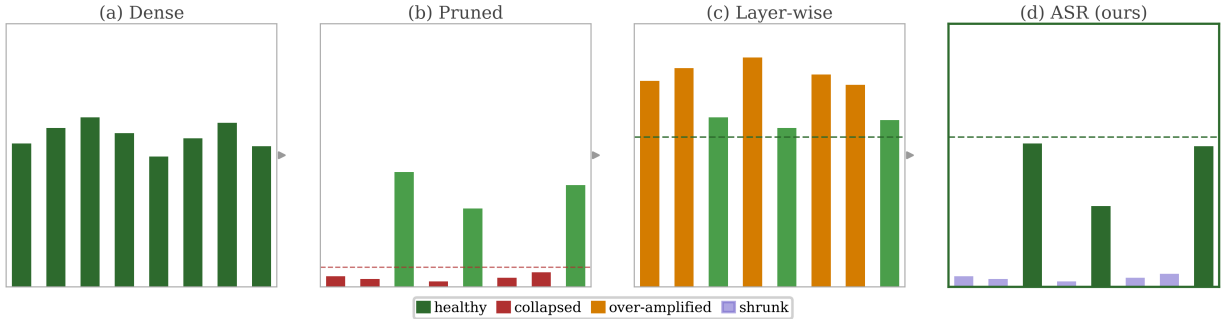


Figure 1: A granularity mismatch in post-pruning repair. Global pruning creates heterogeneous channel damage within a layer. Layer-wise repair applies one shared correction and can over-amplify collapsed channels, whereas ASR applies shrinkage-stabilised channel-wise repair.

boundaries. As a result, the surviving weight density can vary sharply across channels within the same layer: some channels retain much of their original mass, while others lose nearly all of it. This heterogeneous damage causes intermediate activation statistics to shift non-uniformly across channels and depth, gradually weakening the signal needed for reliable prediction [40].

Repairing this shift without retraining is difficult. A simple baseline is BatchNorm recalibration, which updates running mean and variance statistics on a small calibration set after pruning and can recover a substantial part of the lost accuracy [18]. A natural extension is to apply layer-wise activation scaling before BatchNorm recalibration, matching the variance of each pruned layer to that of its dense counterpart, as in the recently proposed REFLOW [40]. This layer-wise strategy, however, assumes that pruning damage is approximately uniform within each layer. Under global pruning, that assumption is systematically violated. Severely damaged and relatively healthy channels can coexist within the same layer, yet a layer-wise correction applies a shared scalar to all of them. When collapsed channels contribute disproportionately to the layer-wise variance ratio, the resulting scalar can become overly large and amplify damaged channels instead of restoring useful signal. Layer-wise repair can therefore become less stable than BatchNorm recalibration alone in the high-sparsity regime where repair is most needed. Figure 1 illustrates this granularity mismatch.

We propose Adaptive Signal Resuscitation (ASR), a training-free post-pruning repair method that matches the granularity of repair to the granularity of damage. For each output channel, ASR estimates a scaling factor from the ratio between dense and pruned activation variance on a small calibration set, and stabilises this estimate through a data-driven shrinkage rule. Channels whose variance has collapsed toward zero receive a correction close to the identity, while channels with healthier variance retain a stronger correction. This adaptive suppression prevents the over-amplification of damaged channels that can destabilise layer-wise scaling. Applied before BatchNorm recalibration, ASR stabilises the activations entering BN layers and improves early calibration efficiency, allowing strong accuracy recovery with fewer recalibration batches.

Our work makes three contributions. We first identify a failure mode of layer-wise activation repair in high-sparsity pruning: when channel damage is highly uneven, a shared layer-wise correction can be driven by collapsed channels and may reduce accuracy below BatchNorm recalibration alone. We then introduce ASR, a training-free channel-wise repair method that uses a data-driven shrinkage rule to suppress unreliable corrections for collapsed channels while retaining stronger corrections for channels with recoverable signal. Finally, we show across CNN vision benchmarks that ASR is most beneficial when pruning damage is severe and heterogeneous, and that applying ASR before BatchNorm recalibration improves recovery under small calibration budgets. ASR estimates its repair factors from 64 calibration images using forward evaluation only; the repaired model is evaluated under the same BatchNorm recalibration budget as the baselines. The method is designed for convolutional networks with BatchNorm. Extensions to transformer architectures and

post-training quantization are left for future work. Additional derivations and diagnostics are provided in Supplementary Sections A–C.4.

2 Related Work

A large body of work on neural network pruning studies which weights, channels, or filters should be removed from a trained model while preserving predictive performance. Classical saliency-based methods estimate the importance of weights or connections before removal [24, 10], while magnitude pruning remains a widely used practical baseline [9]. In vision models, both unstructured and structured pruning have been studied, including filter pruning, channel pruning, and sparsity-inducing normalisation methods [27, 13, 33, 44, 30, 43, 12, 29, 36, 31]. More recent methods exploit richer information than weight magnitude alone [6]. SparseGPT [7] uses approximate second-order updates to compensate surviving weights, Wanda [42] combines weight magnitude with activation statistics, and LAMP [25] allocates sparsity across layers through a model-level distortion criterion. These methods primarily decide which weights to remove, how to allocate sparsity, or how to update the surviving weights. Our work addresses a different stage: given a fixed pruning mask and fixed surviving weights, we study how to repair the activation distribution after pruning without retraining.

Closer to our setting is work on post-pruning signal degradation and calibration-based repair [26, 23]. One-shot pruning can induce progressive variance decay across layers, leading to signal collapse [40]. A natural post-hoc repair strategy is therefore to restore layer-wise activation variance from a small calibration set, without updating trainable weights; the REFLOW preprint [40] is a recent example of this idea. Related activation renormalisation methods also appear outside pruning, for example in REPAIR [21], which corrects preactivation statistics when interpolating or merging networks.

These methods share a calibration-based and training-free philosophy, but their repair granularity is not designed for the heterogeneous channel collapse caused by global magnitude pruning. In our setting, healthy and near-dead channels can coexist within the same layer, so a shared correction can be dominated by collapsed channels and may over-amplify unreliable signal. ASR keeps the same post-hoc repair setting, but adapts activation-statistic repair to this pruning-specific regime by estimating corrections separately for each output channel and shrinking unreliable corrections toward the identity. This distinction is important: our ablation in Table 2 shows that raw channel-wise variance matching is not sufficient. The contribution is therefore not channel granularity alone, but shrinkage-stabilised channel-wise repair for collapsed activations.

ASR uses a data-driven shrinkage rule as a post-hoc reliability weight: after pruning, each channel-wise correction is contracted toward the identity in proportion to how little post-pruning variance the channel retains, so that collapsed channels receive minimal adjustment while healthier channels are corrected more strongly. This differs from the role of James–Stein shrinkage [20] and Bayesian shrinkage priors used for regularisation or compression [19, 32, 35], where shrinkage is applied during training to induce sparsity in weights or posteriors. We do not impose a prior on weights or learn a sparse posterior. In this sense, ASR belongs to the broader family of small-calibration-set correction methods used in post-training quantization and pruning [38, 2, 37, 17, 28, 16, 23], but focuses on a specific failure mode in high-sparsity convolutional networks with BatchNorm: layer-wise repair can become unstable when channel damage is highly heterogeneous.

3 Adaptive Signal Resuscitation

Figure 2 summarises the ASR pipeline. Given a dense model and its pruned counterpart, ASR uses a small calibration set to measure pre-BatchNorm activation statistics, computes a channel-wise repair factor for each convolutional output channel, shrinks unreliable corrections toward the identity, and then recalibrates

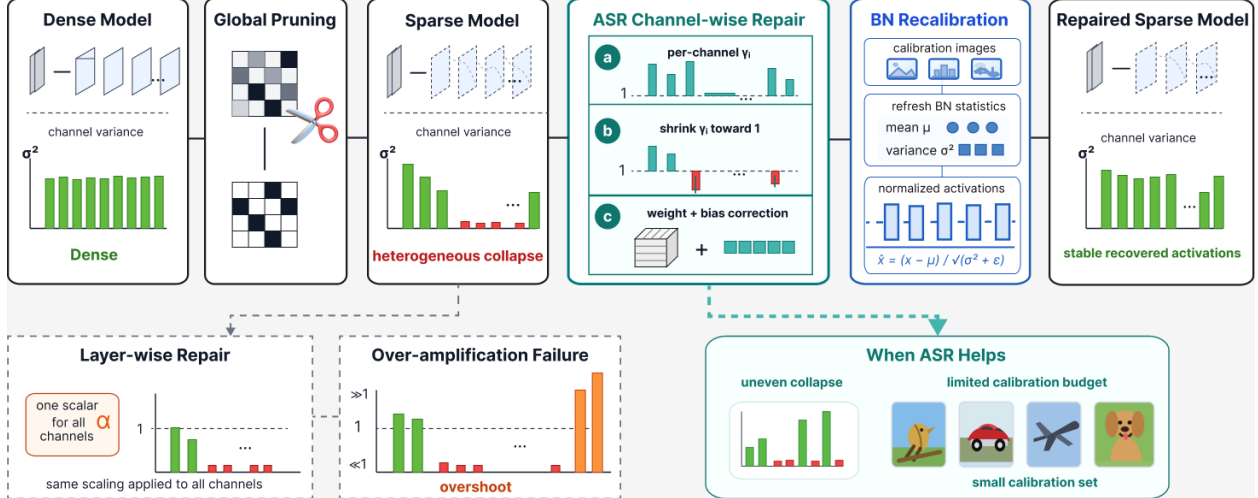


Figure 2: Overview of ASR. ASR repairs heterogeneous post-pruning channel collapse by applying shrinkage-stabilised channel-wise correction before BatchNorm recalibration.

BatchNorm statistics under the repaired activation distribution. We first review why a layer-wise correction can become unstable, then derive the channel-wise variance-matching estimator, and finally introduce the shrinkage and bias-correction steps used by ASR.

3.1 From Layer-wise Repair to Channel-wise Matching

Let $\mathbf{Y}_d \in \mathbb{R}^{N \times C \times H \times W}$ and $\mathbf{Y}_p \in \mathbb{R}^{N \times C \times H \times W}$ denote the pre-BatchNorm output activations of a convolutional layer in the dense and pruned models, respectively, evaluated on a calibration set of N images. For each output channel $i \in \{1, \dots, C\}$, define

$$v_{d,i} = \text{Var}(\mathbf{Y}_{d,i}), \quad v_{p,i} = \text{Var}(\mathbf{Y}_{p,i}),$$

where variance is taken over the batch and spatial dimensions.

A layer-wise repair estimates one correction factor for the whole layer,

$$\gamma_{\text{LW}} = \sqrt{\frac{\frac{1}{C} \sum_{i=1}^C \widehat{\text{Var}}(\mathbf{Y}_{d,i})}{\frac{1}{C} \sum_{i=1}^C \widehat{\text{Var}}(\mathbf{Y}_{p,i}) + \epsilon}}. \quad (1)$$

This estimator is reasonable when post-pruning damage is relatively homogeneous within the layer. Under global magnitude pruning, however, a subset of channels can have near-zero post-pruning variance while other channels remain active. These near-collapsed channels reduce the denominator of the layer-wise ratio, but they do not necessarily contain recoverable signal. The resulting shared correction can therefore become too large and is applied indiscriminately to both healthy and damaged channels. This motivates a repair rule whose correction strength is estimated and stabilised at channel granularity.

If the pruned channel is rescaled by a scalar γ_i , then its variance becomes

$$\text{Var}(\gamma_i \mathbf{Y}_{p,i}) = \gamma_i^2 v_{p,i}.$$

A natural moment-matching objective is therefore to choose γ_i so that the repaired pruned variance is close to the corresponding dense variance. We formalise this by the channel-wise criterion

$$\mathcal{L}_i(\gamma_i) = (\gamma_i^2 v_{p,i} - v_{d,i})^2. \quad (2)$$

Minimising (2) over $\gamma_i \geq 0$ yields the population target

$$\gamma_i^* = \sqrt{\frac{v_{d,i}}{v_{p,i}}}. \quad (3)$$

The non-negativity constraint $\gamma_i \geq 0$ ensures a unique minimiser: the objective (2) is convex in γ_i^2 , so the positive square root is the global minimum over the feasible set, provided $v_{d,i} > 0$.

Replacing population variances by sample variances from the calibration set gives the raw variance-matching estimator

$$\hat{\gamma}_i = \sqrt{\frac{\widehat{\text{Var}}(\mathbf{Y}_{d,i})}{\widehat{\text{Var}}(\mathbf{Y}_{p,i}) + \epsilon}}, \quad (4)$$

where $\epsilon > 0$ is a numerical floor.

Equation (4) is well motivated when $\widehat{\text{Var}}(\mathbf{Y}_{p,i})$ is stably estimated. Under high sparsity, however, some channels may become severely damaged after global pruning, and their post-pruning variances can approach zero. In that regime, the denominator in (4) becomes small, making the raw correction factor unstable. Thus, channel granularity alone is not sufficient: the raw estimator is least reliable for the channels that are most severely damaged, and applying it directly may amplify residual noise instead of restoring useful signal.

3.2 Empirical Bayes Shrinkage Toward the Identity

To stabilise the channel-wise corrections, we introduce a data-driven shrinkage step that contracts unreliable estimates toward the identity map $\gamma_i = 1$. The shrinkage baseline is chosen from the empirical distribution of post-pruning channel variances within the layer:

$$\lambda = \text{median}\left(\left\{\widehat{\text{Var}}(\mathbf{Y}_{p,i})\right\}_{i=1}^C\right). \quad (5)$$

We use the median as the default layer-level shrinkage baseline because it is less sensitive to anomalous channel variances than the mean and performs well in the high-sparsity regime studied in our ablation.

We then define the shrinkage weight

$$s_i = \frac{\widehat{\text{Var}}(\mathbf{Y}_{p,i})}{\widehat{\text{Var}}(\mathbf{Y}_{p,i}) + \lambda}, \quad 0 \leq s_i < 1, \quad (6)$$

and the final repair factor

$$\gamma_i = s_i \hat{\gamma}_i + (1 - s_i) \cdot 1. \quad (7)$$

Equivalently,

$$\gamma_i - 1 = s_i(\hat{\gamma}_i - 1), \quad (8)$$

so γ_i always lies between the raw estimate $\hat{\gamma}_i$ and the identity correction 1. The identity correction is a conservative target: ASR does not attempt to revive a channel whose post-pruning activation has nearly vanished, since such a channel is more likely to carry amplified residual noise than useful signal.

The behaviour of (7) follows directly from (6). If $\widehat{\text{Var}}(\mathbf{Y}_{p,i}) \rightarrow 0$, then $s_i \rightarrow 0$ and

$$\gamma_i \rightarrow 1,$$

so the method applies little or no multiplicative correction to a nearly collapsed channel. If $\widehat{\text{Var}}(\mathbf{Y}_{p,i}) \gg \lambda$, then $s_i \rightarrow 1$ and

$$\gamma_i \rightarrow \hat{\gamma}_i,$$

so the estimator approaches the full variance-matching correction. In this sense, s_i acts as a continuous reliability weight derived from the observed post-pruning activation scale of each channel.

For a convolutional kernel $\mathbf{W}_\ell \in \mathbb{R}^{C_{\text{out}} \times C_{\text{in}} \times k \times k}$, the repair is applied per output channel:

$$\widetilde{\mathbf{W}}_{\ell, i, :, :, :} = \gamma_i \mathbf{W}_{\ell, i, :, :, :}, \quad i = 1, \dots, C_{\text{out}}. \quad (9)$$

Thus each output channel is repaired by a scale factor determined by its own post-pruning activation statistics rather than by a layer-wide average.

3.3 Bias Correction and BatchNorm Recalibration

Pruning can shift activation means as well as variances [38]. After channel-wise rescaling, we optionally adjust the bias so that the repaired pruned activations match the dense activations at the first moment. Let $\gamma = (\gamma_1, \dots, \gamma_C)^\top$ and denote by $\widehat{\mathbb{E}}[\mathbf{Y}_d]$ and $\widehat{\mathbb{E}}[\mathbf{Y}_p]$ the per-channel sample means over the batch and spatial dimensions. If the repaired pre-BN activations are written as

$$\widetilde{\mathbf{Y}}_p = \gamma \odot \mathbf{Y}_p + (\mathbf{b}_{\text{new}} - \mathbf{b}_{\text{old}}),$$

then imposing the moment-matching condition

$$\widehat{\mathbb{E}}[\widetilde{\mathbf{Y}}_p] = \widehat{\mathbb{E}}[\mathbf{Y}_d]$$

gives

$$\mathbf{b}_{\text{new}} = \mathbf{b}_{\text{old}} + \widehat{\mathbb{E}}[\mathbf{Y}_d] - \gamma \odot \widehat{\mathbb{E}}[\mathbf{Y}_p]. \quad (10)$$

This correction aligns the first moment after multiplicative repair, addressing the mean shift that pruning introduces independently of the variance distortion.

For networks with BatchNorm layers, we apply ASR before BatchNorm recalibration. The channel-wise rescaling and bias adjustment first repair the pre-BN activation distribution, after which the BatchNorm running statistics are recomputed on the calibration set. This ordering separates two roles: ASR repairs the convolutional signal at channel granularity, while BatchNorm recalibration updates the downstream normalisation statistics under the repaired activation distribution.

The full ASR procedure requires only forward passes on the calibration set to collect activation statistics, followed by deterministic weight and bias updates. It uses no gradient computation and does not retrain the sparse model. Supplementary Section A gives the corresponding activation-shift derivation and a formal stability view of the shrinkage rule.

4 Experiments

We design the experiments to evaluate whether ASR addresses the failure mode identified above: unstable layer-wise repair under heterogeneous channel damage. In particular, we ask whether ASR improves over layer-wise repair in high-sparsity regimes, whether the effect persists across architectures and datasets, and whether applying ASR before BatchNorm recalibration improves accuracy recovery under limited calibration budgets.

We evaluate ASR across three datasets, four architectures, four pruning conditions, and three repair methods. The datasets are CIFAR-10, CIFAR-100 [22], and Imagenette [14], covering different levels of task difficulty and class granularity. The architectures are ResNet-18, ResNet-50 [11], DenseNet-121 [15], and VGG-16-BN [41], which span different depths, connectivity patterns, and BatchNorm densities. All models are initialised from ImageNet-pretrained weights [4] and fine-tuned for five epochs on the target dataset, with

Algorithm 1: Adaptive Signal Resuscitation (ASR)

Input : Dense model f_d ; pruned model f_p ; calibration set $\mathcal{X} = \{x_n\}_{n=1}^N$
Hyperparam : Numerical floor $\epsilon > 0$
Output : Repaired pruned model f_p

// Stage 1: Channel-wise data-driven shrinkage repair

```
1 foreach convolutional layer  $\ell = 2, \dots, L$  do
    // layer 1 skipped: its input is raw pixels, whose statistics
    // are independent of pruning and require no repair
2 collect pre-BN activations  $\mathbf{Y}_d \leftarrow f_d^{(\ell)}(\mathcal{X})$  and  $\mathbf{Y}_p \leftarrow f_p^{(\ell)}(\mathcal{X})$   $\triangleright \in \mathbb{R}^{N \times C \times H \times W}$ 
3 for  $i = 1$  to  $C$  do
4      $v_{d,i} \leftarrow \widehat{\text{Var}}(\mathbf{Y}_{d,i})$   $\triangleright$  dense channel variance
5      $v_{p,i} \leftarrow \widehat{\text{Var}}(\mathbf{Y}_{p,i})$   $\triangleright$  pruned channel variance
6      $\hat{\gamma}_i \leftarrow \sqrt{v_{d,i}/(v_{p,i} + \epsilon)}$   $\triangleright$  raw variance-matching correction
7 end
8  $\lambda \leftarrow \text{median}(\{v_{p,i}\}_{i=1}^C)$   $\triangleright$  data-driven shrinkage baseline
9 for  $i = 1$  to  $C$  do
10      $s_i \leftarrow v_{p,i}/(v_{p,i} + \lambda)$   $\triangleright$  shrinkage weight
11      $\gamma_i \leftarrow s_i \hat{\gamma}_i + (1 - s_i)$   $\triangleright$  shrunk correction
12 end
13 rescale output-channel filters:  $\mathbf{W}_{\ell,i,:,:,} \leftarrow \gamma_i \mathbf{W}_{\ell,i,:,:,}$  for  $i = 1, \dots, C$   $\triangleright$  channel-wise
    weight repair
14  $\boldsymbol{\mu}_d \leftarrow \widehat{\mathbb{E}}[\mathbf{Y}_d]$  and  $\boldsymbol{\mu}_p \leftarrow \widehat{\mathbb{E}}[\mathbf{Y}_p]$   $\triangleright$  per-channel means
15  $\mathbf{b}_\ell \leftarrow \mathbf{b}_\ell + \boldsymbol{\mu}_d - \gamma \odot \boldsymbol{\mu}_p$   $\triangleright$  bias correction
16 end
```

// Stage 2: BatchNorm recalibration

```
17 Re-estimate BatchNorm running statistics of  $f_p$  on  $\mathcal{X}$ 
18 return  $f_p$ 
```

all layers frozen except the final residual block and classification head. This protocol creates a controlled post-training pruning setting while keeping most of the pretrained visual representation fixed.

We consider global unstructured L1 magnitude pruning at 50%, 70%, and 90% sparsity, implemented with `torch.nn.utils.prune.global_unstructured`, as well as structured 2:4 (N:M) sparsity [34, 46, 16]. After pruning, masks are made permanent before any repair is applied. We compare three post-pruning repair strategies. BN Only resets and re-estimates BatchNorm running mean and variance statistics on a calibration set. LW+BN applies layer-wise activation scaling in the style of REFLOW [40] before the same BatchNorm recalibration. ASR+BN applies our channel-wise shrinkage-stabilised repair before BatchNorm recalibration. We also report the unpruned dense model and the unrepaired pruned model as upper and lower reference points.

ASR estimates its channel-wise correction factors from a small calibration subset of 64 training images. After this repair step, we study BatchNorm recalibration efficiency by varying the number of recalibration batches over $\{10, 20, 30, 50\}$ with batch size 128, and report top-1 test accuracy as a function of calibration budget. All calibration images are drawn from the training set and are disjoint from the test set. Unless

otherwise stated, main results are reported at recalibration step $b = 20$, which provides an early but stable operating point for comparing repair methods. Experiments are run on a single NVIDIA T4 GPU.

Implementation details. All repair methods are applied after the pruning mask has been fixed; none changes the sparsity pattern or performs gradient-based fine-tuning. ASR estimates its channel-wise repair factors using 64 training images. BatchNorm recalibration uses the calibration budget specified in each experiment, and all repair methods are evaluated under the same recalibration budget. Calibration images are sampled from the training set and are disjoint from the test set. Results use a fixed pruning and calibration seed for controlled comparison across repair methods. Supplementary Section B provides the empirical rationale for reporting the main comparison at $b=20$.

5 Results

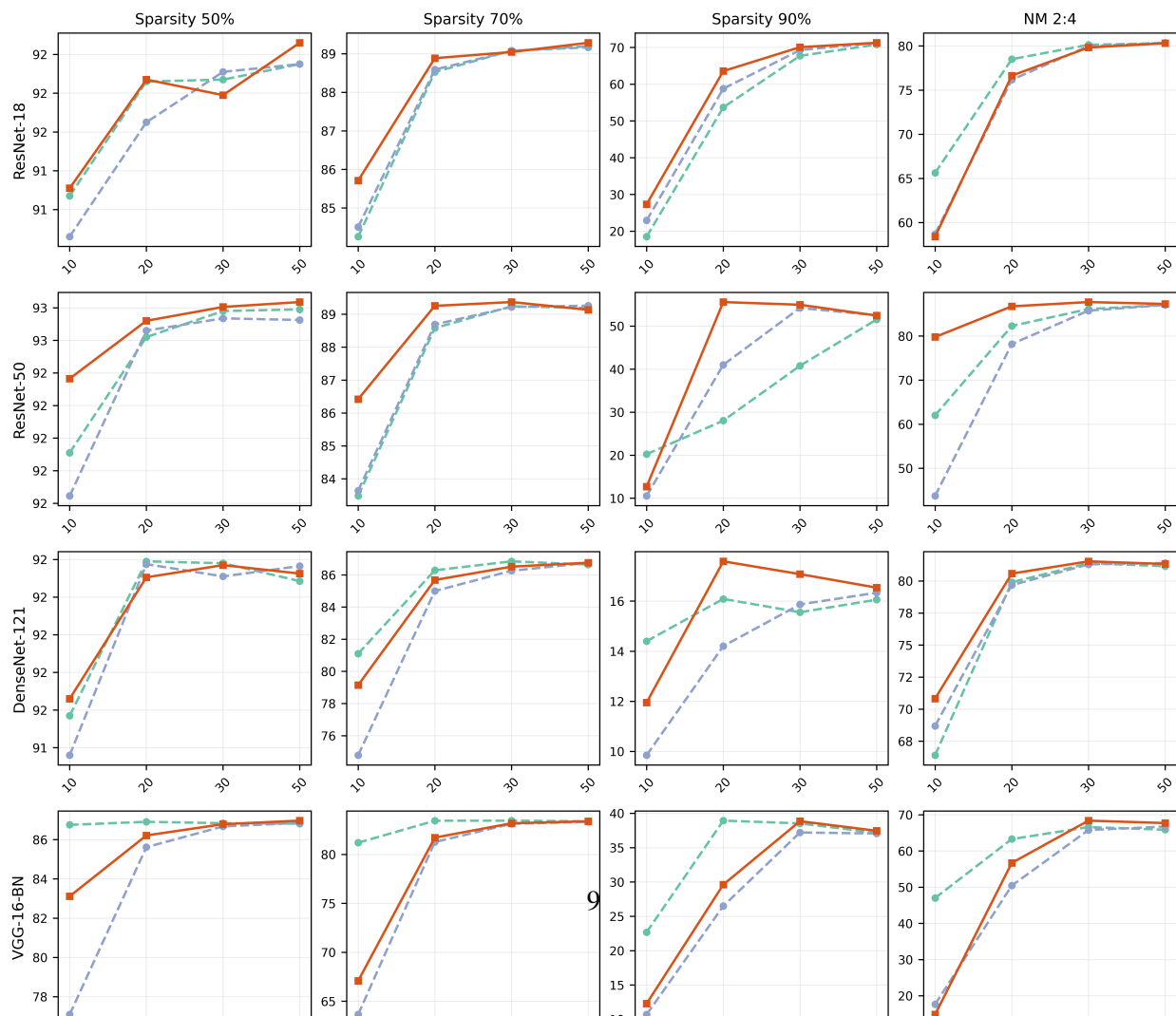
5.1 Main Results

Table 1 reports top-1 test accuracy at calibration step $b=20$ across all architecture, dataset, and pruning combinations. Figure 3 shows the corresponding accuracy trajectories across calibration batch sizes on CIFAR-10. A recurring pattern across settings is the instability of layer-wise scaling at high sparsity. In multiple configurations, LW+BN underperforms the simpler BN-only baseline, which is consistent with the view that a single per-layer scalar can be overly influenced by severely damaged channels and therefore over-correct the repaired activations. The effect is most pronounced on VGG-16-BN at 90% sparsity, where LW+BN falls more than 12 percentage points below BN-only on CIFAR-10 and nearly 9 points on CIFAR-100. A similar pattern appears on DenseNet-121, where LW+BN underperforms BN-only at 90% sparsity across all three datasets. DenseNet’s dense connectivity causes each layer’s output to be concatenated with all preceding feature maps, so weight density—and therefore channel variance—varies more sharply across layers under global pruning than in residual networks; this may compound the variance distortion that layer-wise repair struggles to correct.

ASR+BN usually improves over LW+BN, with the largest gains appearing at the highest sparsity levels. The largest absolute gain over LW+BN occurs on ResNet-50 at 90% sparsity on CIFAR-10, where ASR+BN reaches 55.59% compared to 41.01% for LW+BN, an improvement of 14.58 percentage points. At lower sparsities, where channel collapse is milder and more homogeneous, the differences between repair methods are correspondingly smaller. This pattern suggests that the main benefit of ASR is not stronger rescaling alone, but selective rescaling in settings where channel damage is highly uneven.

Table 1: Top-1 accuracy (%) at calibration step $b=20$, batch size 128. Bold indicates the best result among repair methods at each setting. The unrepaired pruned model is shown in gray for reference. Results are shown for sparsity levels 70%, 90%, and NM 2:4; 50% results are omitted because all repair methods perform similarly at low sparsity.

Architecture	Method	CIFAR-10			CIFAR-100			Imagenette		
		70%	90%	2:4	70%	90%	2:4	70%	90%	2:4
ResNet-18	Dense		92.77			75.56			97.27	
	No Repair	37.73	8.19	15.68	3.20	1.00	3.83	92.60	11.12	32.33
	BN Only	88.53	53.70	78.50	60.45	15.55	48.75	96.69	90.04	91.59
	LW+BN	88.59	58.77	76.17	60.36	7.10	44.46	96.69	91.06	92.22
	ASR+BN	88.88	63.56	76.64	60.75	15.25	46.39	96.73	91.68	92.47
ResNet-50	Dense		93.33			75.05			98.22	
	No Repair	10.87	10.00	13.55	1.17	1.00	2.31	93.22	22.05	37.18
	BN Only	88.58	28.04	82.28	58.18	4.01	57.22	97.52	86.39	93.92
	LW+BN	88.69	41.01	78.18	58.02	5.04	51.06	97.68	66.15	95.31
	ASR+BN	89.25	55.59	86.74	58.80	6.88	60.75	97.68	82.98	95.67
DenseNet-121	Dense		92.75			75.11			98.88	
	No Repair	40.74	9.29	12.57	8.86	0.93	2.16	78.90	14.79	49.97
	BN Only	86.28	16.09	79.91	62.09	1.96	53.17	97.34	73.10	95.87
	LW+BN	85.00	14.21	79.68	58.84	2.25	53.31	96.75	29.54	95.44
	ASR+BN	85.68	17.59	80.58	60.65	2.99	54.00	97.10	44.13	96.25
VGG-16-BN	Dense		87.35			64.61			98.50	
	No Repair	52.15	11.90	14.72	24.26	1.34	5.03	92.20	15.86	62.99
	BN Only	83.44	38.93	63.29	57.72	14.74	35.50	97.41	70.29	94.10
	LW+BN	81.27	26.49	50.43	53.02	6.06	21.59	96.89	47.43	94.25
	ASR+BN	81.72	29.62	56.70	53.27	5.89	27.15	97.06	52.04	94.05



The comparison between ASR+BN and BN-only is more nuanced. On ResNet-18 and ResNet-50, ASR+BN matches or exceeds BN-only in most high-sparsity settings. On VGG-16-BN, however, BN-only outperforms both LW+BN and ASR+BN at 90% sparsity and under NM 2:4 sparsity. VGG-16-BN lacks residual connections, so activation signal cannot bypass collapsed layers; when a large fraction of channels approach zero variance, even shrinkage-stabilised corrections operate on a distribution that carries little recoverable information. In this regime, multiplicative repair at any granularity appears to introduce more instability than it resolves, and BatchNorm recalibration alone—which makes no multiplicative adjustment to the convolutional weights—proves the more conservative and reliable strategy. Whether channel-wise repair can be further stabilised in very deep networks without skip connections remains an open question. On Imagenette, where the fine-tuned dense model is already close to ceiling performance, all three repair methods perform more similarly, consistent with a setting in which the post-pruning damage is less severe.

Figure 3 also shows that the advantage of ASR+BN over LW+BN is most visible at small calibration budgets, especially at $b=10$ and $b=20$. In this regime, repairing convolutional weights before BatchNorm recalibration appears to stabilise the activations entering BN layers and thereby improve early calibration efficiency. As b increases, the gap between methods narrows and performance tends to approach a common ceiling, consistent with BatchNorm statistics becoming better estimated across all repair strategies.

5.2 Mechanism: Channel-wise Variance Repair

Figure 4 visualises per-channel activation variance after each repair method for ResNet-50 on CIFAR-10 with NM 2:4 sparsity. The channels are sorted by dense variance, and each repaired variance is compared against the dense reference. The ideal repair corresponds to a log-log slope $\alpha = 1$, meaning that repaired variance tracks the dense reference proportionally across all channels; a slope above one indicates systematic over-correction, and a slope below one indicates under-correction.

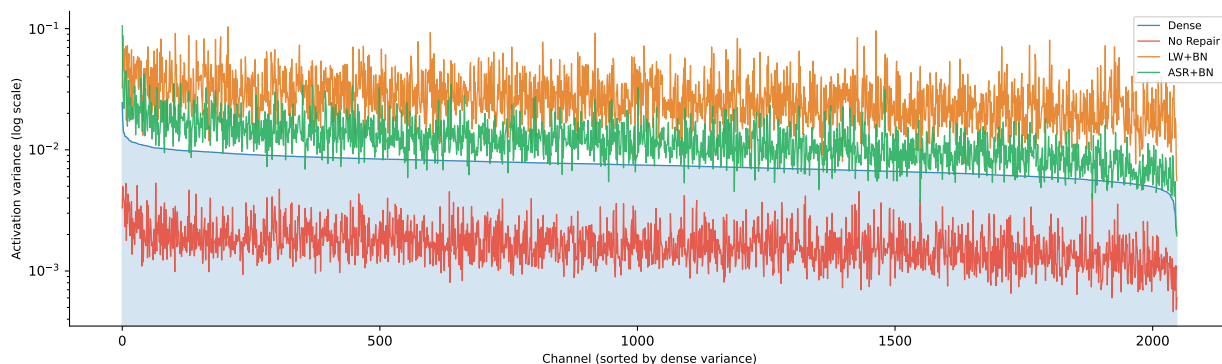


Figure 4: Per-channel activation variance after repair for ResNet-50 on CIFAR-10 with NM 2:4 sparsity at `layer4.0.conv3`. The dense curve is the reference. No Repair remains under-corrected ($\alpha = 0.23$), LW+BN over-corrects ($\alpha = 3.84$), and ASR+BN is closer to the dense target ($\alpha = 1.68$).

The pruned model remains strongly under-corrected ($\alpha = 0.23$), with most channels lying well below the dense level. Layer-wise scaling moves in the opposite direction and substantially over-corrects the activations ($\alpha = 3.84$), pushing many channel variances above the dense reference; a slope well above one means that channels with low post-pruning variance receive the same large multiplicative correction as healthy channels, amplifying noise rather than signal. ASR+BN produces a slope closer to the ideal value ($\alpha = 1.68$), indicating a more moderate correction that is better aligned with the dense target. This tighter variance alignment translates directly into the accuracy differences observed in Table 1: on ResNet-50 at

NM 2:4 sparsity, ASR+BN reaches 86.74% on CIFAR-10 compared with 82.28% for BN-only and 78.18% for LW+BN, a gap that is consistent with the over-correction visible in Figure 4. More broadly, this pattern confirms the argument in Section 3: a single layer-wise scalar is too coarse to reflect the heterogeneous damage induced by global pruning, whereas channel-wise correction with shrinkage yields a more stable repair.

Figure 5 gives a spatial view of the same failure mode. After pruning, the feature response is weakened; after layer-wise repair, the response can be over-amplified relative to the dense reference. ASR+BN produces activation maps that are visually closer to the dense model, consistent with its more selective channel-wise correction. Supplementary Section C.3 provides layer-wise heatmaps that show the same over-correction pattern across representative networks.

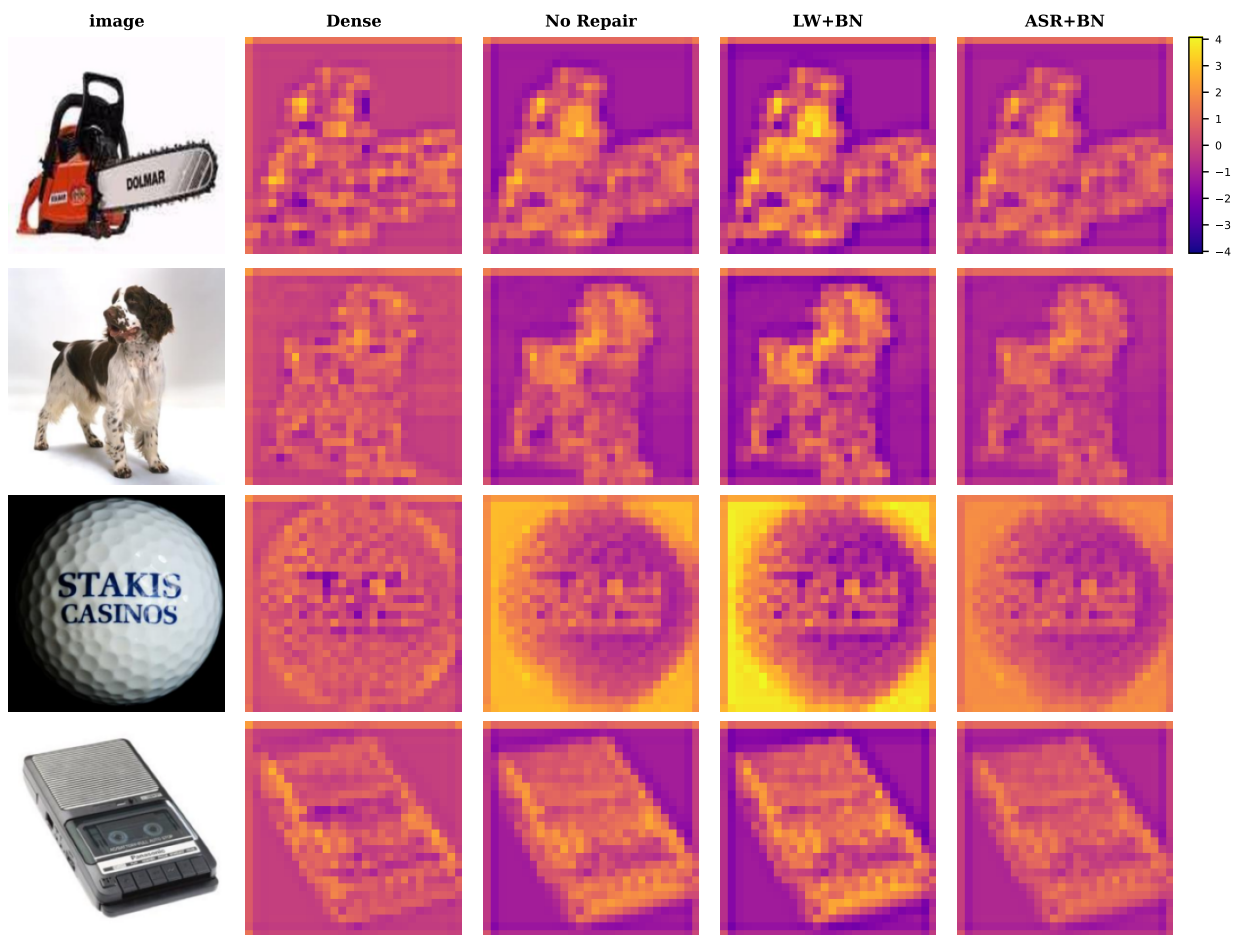


Figure 5: Spatial activation maps at `layer2.0.conv1`, channel 1 of ResNet-18 on Imagenette under 90% global L1 sparsity. Each row corresponds to a different test image. Pruning weakens the feature response, LW+BN over-amplifies it relative to the dense reference, and ASR+BN recovers a spatial pattern closer to the dense activation.

5.3 When Does ASR Help?

The results above suggest that ASR is most useful when pruning induces severe channel-wise variance distortion. We quantify this relationship by comparing the accuracy gain of ASR+BN over LW+BN at calibration step $b=20$ against a pruning-severity statistic computed from channel-wise variance ratios. As

shown in Figure 6, larger deviation of pruned channel variances from the dense reference is associated with a larger ASR advantage over layer-wise repair, with Pearson correlation $r = 0.61$ and Spearman correlation $\rho = 0.70$.

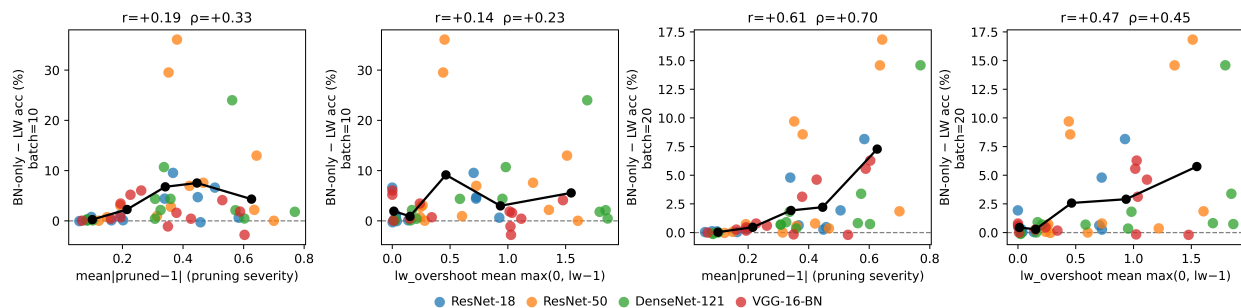


Figure 6: Accuracy gain of ASR+BN over LW+BN versus pruning severity (average channel variance deviation from the dense reference) at calibration step $b=20$. Each point is one architecture–dataset–sparsity combination. Larger severity is associated with larger ASR advantage ($r = 0.61$, $\rho = 0.70$).

This trend is consistent with the mechanism proposed in Section 3. When channel damage is mild, a shared layer-wise correction is often sufficient and the gain from ASR is small. As post-pruning channel variances become more distorted, however, the layer-wise scalar becomes increasingly mismatched to the heterogeneous channel state. In this regime, ASR benefits from estimating correction strength at channel granularity and shrinking unreliable corrections toward the identity. A small number of points in Figure 6 fall near or marginally below zero, corresponding to low-severity settings where the two methods perform comparably; these are concentrated at pruning severity below 0.2, where channel collapse is mild enough that a shared scalar already captures most of the needed correction.

5.4 Ablation Study

Table 2 isolates the contributions of channel granularity, data-driven shrinkage, and bias correction under a representative high-sparsity setting. We compare BN only, layer-wise repair, raw channel-wise variance matching without shrinkage, and several ASR variants. This ablation separates three effects: whether channel granularity alone is sufficient, whether shrinkage stabilises raw channel-wise correction, and whether bias correction provides an additional gain once shrinkage is used.

The results show that channel granularity alone is not sufficient in this setting. Moving from layer-wise repair to raw channel-wise repair does not improve accuracy, indicating that naive channel-wise correction remains unstable at high sparsity. Adding shrinkage leads to a large gain: the fixed-prior ASR variant already improves over both layer-wise and raw channel-wise repair, while the adaptive variants perform substantially better. Among them, the best result is achieved by ASR with a median prior and bias correction. The mean-prior variant is also strong, and the gap between the median-prior variants with and without bias correction is relatively small, suggesting that the choice of prior has a secondary effect once the shrinkage mechanism is in place. Taken together, these results confirm that the main benefit of ASR comes from stabilised channel-wise repair, while bias correction plays a supporting role.

Table 2: Ablation on ResNet-50/CIFAR-10 at 90% sparsity. Top-1 accuracy (%) is reported for layer-wise repair, raw channel-wise repair, and ASR variants.

Method	Accuracy
BN only	29.11
Layer-wise + BN	39.42
Channel-wise raw + BN	29.30
ASR, fixed prior	45.24
ASR, median prior	52.26
ASR, mean prior + bias correction	53.95
ASR, median prior + bias correction	55.59

This ablation clarifies why ASR is not simply direct activation renormalisation at a finer granularity. Moving from layer-wise to raw channel-wise matching is insufficient because collapsed channels make unshrunk variance ratios unreliable. The gain appears when channel-wise repair is made reliability-aware through shrinkage. ASR is therefore a collapse-aware repair rule for fixed sparse models, rather than a stronger form of unconstrained activation matching.

6 Conclusion

We have presented Adaptive Signal Resuscitation (ASR), a training-free post-pruning repair method for activation distribution shift in sparse vision networks. The central observation is that post-pruning damage is not uniformly distributed within a layer. Under global magnitude pruning, severely collapsed channels can coexist with channels that retain informative activation variance, making a single layer-wise correction too coarse. In this regime, layer-wise scaling can be dominated by collapsed channels and may over-amplify unreliable signal rather than restore useful activations. ASR addresses this granularity mismatch by estimating channel-wise variance-matching corrections and stabilising them with a data-driven shrinkage rule, which pulls unreliable corrections toward the identity while preserving stronger adjustments for channels with sufficient remaining signal.

Across four convolutional architectures, three datasets, and both unstructured and structured sparsity settings, ASR+BN generally improves over layer-wise repair, with the clearest gains in the high-sparsity regimes where repair is most needed. The gains are largest when pruning induces severe channel-wise variance distortion, supporting the view that ASR is most useful when layer-wise repair becomes mismatched to heterogeneous channel damage. We also find that applying ASR before BatchNorm recalibration improves early calibration efficiency, allowing strong accuracy recovery under small calibration budgets without gradient updates or retraining.

7 Limitations and Future Work

The scope of this study points to several natural extensions. ASR requires access to the dense model’s activations during calibration, which matches many post-training compression workflows but may not hold when only a pruned model is retained. Our fine-tuning protocol keeps most pretrained layers fixed, providing a controlled setting for isolating post-pruning repair effects rather than an exhaustive evaluation of all fully fine-tuned deployment pipelines.

The method is designed for convolutional networks with BatchNorm. Extending the same granularity-matched repair principle to architectures with different normalisation mechanisms, such as transformer models with layer normalisation, is a promising direction. The results on VGG-16-BN further suggest that

multiplicative channel-wise repair loses effectiveness when skip connections are absent and channel collapse is especially severe, pointing to an informative boundary case for future repair criteria.

References

- [1] Davis Blalock, Jose Javier Gonzalez Ortiz, Jonathan Frankle, and John Gutttag. What is the state of neural network pruning? *Proceedings of Machine Learning and Systems*, 2:129–146, 2020.
- [2] Yaohui Cai, Zhewei Yao, Zhen Dong, Amir Gholami, Michael W. Mahoney, and Kurt Keutzer. Zeroq: A novel zero shot quantization framework. In *Proceedings of the IEEE/CVF Conference on Computer Vision and Pattern Recognition*, pages 13169–13178, 2020.
- [3] Hongrong Cheng, Miao Zhang, and Javen Qinfeng Shi. A survey on deep neural network pruning: Taxonomy, comparison, analysis, and recommendations. *IEEE Transactions on Pattern Analysis and Machine Intelligence*, 46(12):10558–10578, 2024.
- [4] Jia Deng, Wei Dong, Richard Socher, Li-Jia Li, Kai Li, and Fei-Fei Li. Imagenet: A large-scale hierarchical image database. In *2009 IEEE Computer Society Conference on Computer Vision and Pattern Recognition Workshops*, pages 248–255. IEEE Computer Society, 2009.
- [5] Jonathan Frankle and Michael Carbin. The lottery ticket hypothesis: Finding sparse, trainable neural networks. In *International Conference on Learning Representations*, 2019.
- [6] Elias Frantar and Dan Alistarh. Optimal brain compression: A framework for accurate post-training quantization and pruning. In *Advances in Neural Information Processing Systems*, volume 35, pages 4475–4488. Curran Associates, Inc., 2022.
- [7] Elias Frantar and Dan Alistarh. Sparsegpt: Massive language models can be accurately pruned in one-shot. In *Proceedings of the 40th International Conference on Machine Learning, ICML, 2023*.
- [8] Song Han, Huizi Mao, and William J. Dally. Deep compression: Compressing deep neural networks with pruning, trained quantization and huffman coding. In *International Conference on Learning Representations*, 2016.
- [9] Song Han, Jeff Pool, John Tran, and William J. Dally. Learning both weights and connections for efficient neural networks. In *Advances in Neural Information Processing Systems*, volume 28. Curran Associates, Inc., 2015.
- [10] B. Hassibi, D. G. Stork, and G. J. Wolff. Optimal brain surgeon and general network pruning. In *IEEE International Conference on Neural Networks*, pages 293–299, 1993.
- [11] Kaiming He, Xiangyu Zhang, Shaoqing Ren, and Jian Sun. Deep residual learning for image recognition. In *2016 IEEE Conference on Computer Vision and Pattern Recognition*, pages 770–778. IEEE Computer Society, 2016.
- [12] Yang He, Guoliang Kang, Xuanyi Dong, Yanwei Fu, and Yi Yang. Soft filter pruning for accelerating deep convolutional neural networks. In *Proceedings of the Twenty-Seventh International Joint Conference on Artificial Intelligence*, pages 2234–2240, 2018.
- [13] Yihui He, Xiangyu Zhang, and Jian Sun. Channel pruning for accelerating very deep neural networks. In *2017 IEEE International Conference on Computer Vision*, pages 1398–1406, 2017.
- [14] Jeremy Howard. Imagenette: A smaller subset of 10 easily classified classes from imagenet. <https://github.com/fastai/imagenette>, 2019. Accessed: 2026-05-05.

- [15] Gao Huang, Zhuang Liu, Laurens Van Der Maaten, and Kilian Q. Weinberger. Densely connected convolutional networks. In *Proceedings of the IEEE Conference on Computer Vision and Pattern Recognition*, pages 4700–4708, 2017.
- [16] Itay Hubara, Brian Chmiel, Moshe Isard, Ron Banner, Joseph Naor, and Daniel Soudry. Accelerated sparse neural training: A provable and efficient method to find N:M transposable masks. In *Advances in Neural Information Processing Systems*, volume 34, pages 21099–21111. Curran Associates, Inc., 2021.
- [17] Itay Hubara, Yury Nahshan, Yair Hanani, Ron Banner, and Daniel Soudry. Accurate post training quantization with small calibration sets. In *Proceedings of the 38th International Conference on Machine Learning*, volume 139 of *Proceedings of Machine Learning Research*, pages 4466–4475. PMLR, 2021.
- [18] Sergey Ioffe and Christian Szegedy. Batch normalization: Accelerating deep network training by reducing internal covariate shift. In *Proceedings of the 32nd International Conference on Machine Learning*, volume 37 of *Proceedings of Machine Learning Research*, pages 448–456. PMLR, 2015.
- [19] Hemant Ishwaran and J. Sunil Rao. Spike and slab variable selection: Frequentist and bayesian strategies. *The Annals of Statistics*, 33(2):730–773, 2005.
- [20] William James and Charles Stein. Estimation with quadratic loss. *Proceedings of the Fourth Berkeley Symposium on Mathematical Statistics and Probability*, 1:361–379, 1961.
- [21] Keller Jordan, Hanie Sedghi, Olga Saukh, Rahim Entezari, and Behnam Neyshabur. REPAIR: RENormalizing permuted activations for interpolation repair. In *The Eleventh International Conference on Learning Representations*, 2023.
- [22] Alex Krizhevsky. Learning multiple layers of features from tiny images. Technical report, University of Toronto, 2009.
- [23] Ivan Lazarevich, Alexander Kozlov, and Nikita Malinin. Post-training deep neural network pruning via layer-wise calibration. In *Proceedings of the IEEE/CVF International Conference on Computer Vision Workshops*, pages 798–805, 2021.
- [24] Yann LeCun, John S. Denker, and Sara A. Solla. Optimal brain damage. In *Advances in Neural Information Processing Systems*, volume 2. Morgan-Kaufmann, 1989.
- [25] Jaeho Lee, Sejun Park, Sangwoo Mo, Sungsoo Ahn, and Jinwoo Shin. Layer-adaptive sparsity for the magnitude-based pruning. In *International Conference on Learning Representations*, 2021.
- [26] Bailin Li, Bowen Wu, Jiang Su, and Guangrun Wang. Eagleeye: Fast sub-net evaluation for efficient neural network pruning. In *Computer Vision – ECCV 2020*, volume 12347 of *Lecture Notes in Computer Science*, pages 639–654. Springer, 2020.
- [27] Hao Li, Asim Kadav, Igor Durdanovic, Hanan Samet, and Hans Peter Graf. Pruning filters for efficient convnets. In *International Conference on Learning Representations*, 2017.
- [28] Yuhang Li, Ruihao Gong, Xu Tan, Yang Yang, Peng Hu, Qi Zhang, Fengwei Yu, Wei Wang, and Shi Gu. {BRECQ}: Pushing the limit of post-training quantization by block reconstruction. In *International Conference on Learning Representations*, 2021.
- [29] Shaohui Lin, Rongrong Ji, Chenqian Yan, Baochang Zhang, Liujuan Cao, Qixiang Ye, Feiyue Huang, and David Doermann. Towards optimal structured cnn pruning via generative adversarial learning. In *Proceedings of the IEEE/CVF Conference on Computer Vision and Pattern Recognition*, June 2019.

- [30] Zhuang Liu, Jianguo Li, Zhiqiang Shen, Gao Huang, Shoumeng Yan, and Changshui Zhang. Learning efficient convolutional networks through network slimming. In *2017 IEEE International Conference on Computer Vision*, pages 2755–2763, 2017.
- [31] Zhuang Liu, Mingjie Sun, Tinghui Zhou, Gao Huang, and Trevor Darrell. Rethinking the value of network pruning. In *International Conference on Learning Representations*, 2019.
- [32] Christos Louizos, Karen Ullrich, and Max Welling. Bayesian compression for deep learning. In *Advances in Neural Information Processing Systems*, volume 30. Curran Associates, Inc., 2017.
- [33] Jian-Hao Luo, Jianxin Wu, and Weiyao Lin. Thinet: A filter level pruning method for deep neural network compression. In *2017 IEEE International Conference on Computer Vision*, pages 5068–5076, 2017.
- [34] Asit Mishra, Jorge Albericio Latorre, Jeff Pool, Darko Stosic, Dusan Stosic, Ganesh Venkatesh, Chong Yu, and Paulius Micikevicius. Accelerating sparse deep neural networks, 2021.
- [35] Dmitry Molchanov, Arsenii Ashukha, and Dmitry Vetrov. Variational dropout sparsifies deep neural networks. In *Proceedings of the 34th International Conference on Machine Learning*, volume 70 of *Proceedings of Machine Learning Research*, pages 2498–2507. PMLR, 2017.
- [36] Pavlo Molchanov, Arun Mallya, Stephen Tyree, Iuri Frosio, and Jan Kautz. Importance estimation for neural network pruning. In *2019 IEEE/CVF Conference on Computer Vision and Pattern Recognition*, pages 11256–11264. IEEE Computer Society, 2019.
- [37] Markus Nagel, Rana Ali Amjad, Mart Van Baalen, Christos Louizos, and Tijmen Blankevoort. Up or down? adaptive rounding for post-training quantization. In *Proceedings of the 37th International Conference on Machine Learning*, volume 119 of *Proceedings of Machine Learning Research*, pages 7197–7206. PMLR, 2020.
- [38] Markus Nagel, Mart Van Baalen, Tijmen Blankevoort, and Max Welling. Data-free quantization through weight equalization and bias correction. In *2019 IEEE/CVF International Conference on Computer Vision (ICCV)*, pages 1325–1334, 2019.
- [39] Alex Renda, Jonathan Frankle, and Michael Carbin. Comparing rewinding and fine-tuning in neural network pruning. In *International Conference on Learning Representations*, 2020.
- [40] Dhananjay Saikumar and Blesson Varghese. Signal collapse in one-shot pruning: When sparse models fail to distinguish neural representations, 2025.
- [41] Karen Simonyan and Andrew Zisserman. Very deep convolutional networks for large-scale image recognition. In *International Conference on Learning Representations*, 2015.
- [42] Mingjie Sun, Zhuang Liu, Anna Bair, and J. Zico Kolter. A simple and effective pruning approach for large language models. In *The Twelfth International Conference on Learning Representations*, 2024.
- [43] Huan Wang, Qiming Zhang, Yuehai Wang, and Haoji Hu. Structured probabilistic pruning for convolutional neural network acceleration. In *British Machine Vision Conference*, 2018.
- [44] Wei Wen, Chunpeng Wu, Yandan Wang, Yiran Chen, and Hai Li. Learning structured sparsity in deep neural networks. In *Advances in Neural Information Processing Systems*, volume 29, 2016.

- [45] Tien-Ju Yang, Andrew Howard, Bo Chen, Xiao Zhang, Alec Go, Mark Sandler, Vivienne Sze, and Hartwig Adam. Netadapt: Platform-aware neural network adaptation for mobile applications. In *Proceedings of the European Conference on Computer Vision*, September 2018.
- [46] Aojun Zhou, Yukun Ma, Junnan Zhu, Jianbo Liu, Zhijie Zhang, Kun Yuan, Wenxiu Sun, and Hongsheng Li. Learning n:m fine-grained structured sparse neural networks from scratch. In *International Conference on Learning Representations*, 2021.

A Methodology

This section expands the method introduced in Section 3 of the main paper. We provide additional methodological details for Adaptive Signal Resuscitation (ASR). The main paper presents ASR as a training-free post-pruning repair method that corrects activation distribution shift at channel granularity. This supplement expands the derivation and gives a formal account of why a shared layer-wise correction can become unstable when pruning damage is heterogeneous across channels.

A.1 Activation Distribution Shift from Pruning

Consider a convolutional layer with weight tensor $\mathbf{W} \in \mathbb{R}^{C_{\text{out}} \times C_{\text{in}} \times k \times k}$ and bias $\mathbf{b} \in \mathbb{R}^{C_{\text{out}}}$. Let $\mathbf{m} \in \{0, 1\}^{C_{\text{out}} \times C_{\text{in}} \times k \times k}$ be the binary pruning mask, so the surviving weight is $\widetilde{\mathbf{W}} = \mathbf{m} \odot \mathbf{W}$.

For output channel i , the dense pre-activation on input \mathbf{x} is

$$z_i = \langle \mathbf{w}_i, \mathbf{x} \rangle + b_i, \quad (11)$$

where \mathbf{w}_i denotes the i -th output filter flattened over $C_{\text{in}} \times k \times k$ dimensions. After pruning, the same computation becomes

$$\widetilde{z}_i = \langle \mathbf{m}_i \odot \mathbf{w}_i, \mathbf{x} \rangle + b_i = z_i - \langle (1 - \mathbf{m}_i) \odot \mathbf{w}_i, \mathbf{x} \rangle. \quad (12)$$

Let

$$e_i = \langle (1 - \mathbf{m}_i) \odot \mathbf{w}_i, \mathbf{x} \rangle$$

denote the removed-weight contribution for channel i . The pruning residual depends on both the removed weights and the input patch distribution. Under a simplifying approximation in which input elements are weakly correlated with the removed weights, its variance scales with the removed weight energy,

$$\text{Var}(e_i) \approx \|(1 - \mathbf{m}_i) \odot \mathbf{w}_i\|_2^2 \sigma_x^2, \quad (13)$$

where σ_x^2 denotes an average input variance. This expression is not intended as an exact generative model of pruning damage. Rather, it highlights that channels losing different amounts of weight energy can experience different magnitudes of activation perturbation.

The pruned activation variance can be written as

$$\text{Var}(\widetilde{z}_i) = \text{Var}(z_i - e_i) = \text{Var}(z_i) + \text{Var}(e_i) - 2 \text{Cov}(z_i, e_i). \quad (14)$$

Thus pruning can either contract or distort activation variance depending on the covariance term. In the high-sparsity regimes studied in the main text, we empirically observe that many channels have strongly reduced post-pruning variance, while other channels retain a substantial fraction of their dense activation scale. This non-uniformity is the key point: global magnitude pruning does not enforce uniform damage across channels, so the resulting activation distribution shift can be highly heterogeneous within a single layer.

A.2 Channel-wise Repair with Data-driven Shrinkage

Given dense and pruned pre-BatchNorm activations, a natural local repair is to match the activation variance of each output channel. If a pruned channel is rescaled by a scalar γ_i , its variance becomes

$$\text{Var}(\gamma_i \widetilde{z}_i) = \gamma_i^2 \text{Var}(\widetilde{z}_i).$$

Matching this variance to the dense channel variance gives the population target

$$\gamma_i^* = \sqrt{\frac{\text{Var}(z_i)}{\text{Var}(\tilde{z}_i)}}. \quad (15)$$

Equivalently, γ_i^* minimises

$$(\gamma_i^2 \text{Var}(\tilde{z}_i) - \text{Var}(z_i))^2$$

over $\gamma_i \geq 0$ whenever the variances are positive.

Since the population variances are unknown, ASR estimates them from a small calibration set. Let $\mathbf{Y}_d \in \mathbb{R}^{N \times C \times H \times W}$ and $\mathbf{Y}_p \in \mathbb{R}^{N \times C \times H \times W}$ denote the pre-BatchNorm activations of a layer from the dense and pruned models, computed on N calibration images. The raw channel-wise variance-matching estimator is

$$\hat{\gamma}_i = \sqrt{\frac{\widehat{\text{Var}}(\mathbf{Y}_{d,i})}{\widehat{\text{Var}}(\mathbf{Y}_{p,i}) + \epsilon}}, \quad (16)$$

where the variance is computed over batch and spatial dimensions (n, h, w) , and $\epsilon > 0$ is a numerical floor.

Raw channel-wise matching is unstable for nearly collapsed channels. If $\widehat{\text{Var}}(\mathbf{Y}_{p,i})$ is close to zero, then $\hat{\gamma}_i$ can become large even when the residual activation is mostly noise or numerical fluctuation. A layer-wise correction has the opposite problem: it averages over all channels and applies the same scalar to healthy and damaged channels alike. ASR addresses both issues by estimating the correction at channel granularity and then shrinking unreliable channel-wise estimates toward the identity.

We define a layer-level shrinkage baseline from the empirical distribution of post-pruning channel variances,

$$\lambda = \text{median} \left(\left\{ \widehat{\text{Var}}(\mathbf{Y}_{p,i}) \right\}_{i=1}^C \right). \quad (17)$$

The median is used as a robust layer-level scale. It is less affected than the mean by a small number of anomalously large or small channel variances. We then define

$$s_i = \frac{\widehat{\text{Var}}(\mathbf{Y}_{p,i})}{\widehat{\text{Var}}(\mathbf{Y}_{p,i}) + \lambda}, \quad (18)$$

and set the final ASR correction factor to

$$\gamma_i = s_i \hat{\gamma}_i + (1 - s_i) \cdot 1. \quad (19)$$

Equivalently,

$$\gamma_i - 1 = s_i (\hat{\gamma}_i - 1). \quad (20)$$

This form makes the reliability interpretation explicit. Channels with small post-pruning variance have small s_i and are pulled toward the identity correction. Channels with sufficiently large post-pruning variance have s_i closer to one and retain more of the raw variance-matching correction.

The terminology ‘‘empirical Bayes’’ is used in this limited sense: the shrinkage scale is estimated from the empirical distribution of post-pruning channel variances within the layer, and the resulting rule contracts uncertain channel-wise estimates toward a conservative identity target. We do not perform full Bayesian posterior inference over weights or activations.

The weight update applies the correction per output channel:

$$\widetilde{\mathbf{W}}_{\ell,i,\cdot,\cdot,\cdot} \leftarrow \gamma_i \widetilde{\mathbf{W}}_{\ell,i,\cdot,\cdot,\cdot}, \quad i = 1, \dots, C_{\text{out}}. \quad (21)$$

This is equivalent to multiplying the corresponding pre-BatchNorm output channel by γ_i .

A.3 Formal Stability Analysis

We now formalise the difference between a shared layer-wise correction and the shrinkage-stabilised channel-wise correction used by ASR. The purpose of this analysis is to capture the failure mode observed empirically in the main text, not to claim a complete probabilistic model of pruning.

Sensitivity of layer-wise scaling. Let a layer have C output channels. Denote the post-pruning activation variance of channel i by $v_i = \widehat{\text{Var}}(\mathbf{Y}_{p,i})$, and the average dense activation variance by

$$\bar{v}_d = \frac{1}{C} \sum_{i=1}^C \widehat{\text{Var}}(\mathbf{Y}_{d,i}).$$

Suppose the first k channels are near-dead, so $v_i \leq \delta$ for $i \leq k$, where $\delta > 0$ is small. The layer-wise correction factor is

$$\gamma_{\text{LW}}^2 = \frac{\bar{v}_d}{\frac{1}{C} \left(\sum_{i=1}^k v_i + \sum_{i=k+1}^C v_i \right)}. \quad (22)$$

As $\delta \rightarrow 0$, the contribution of the near-dead channels to the denominator vanishes, and

$$\gamma_{\text{LW}}^2 \rightarrow \frac{C\bar{v}_d}{\sum_{i=k+1}^C v_i}. \quad (23)$$

Equation (23) shows that the shared correction is sensitive to the remaining active variance mass. If many channels are collapsed, or if the remaining active channels have insufficient variance to stabilise the layer average, the layer-wise scalar can grow large. Since the same γ_{LW} is then applied to all channels, the correction cannot distinguish healthy channels from channels whose post-pruning signal is unreliable. This is the granularity mismatch motivating ASR.

Shrinkage property of ASR. For ASR, the correction factor satisfies

$$\gamma_i = s_i \hat{\gamma}_i + (1 - s_i), \quad s_i = \frac{v_i}{v_i + \lambda}.$$

Assume $\lambda > 0$. If channel i is near-dead with $v_i \leq \delta$, then

$$s_i = \frac{v_i}{v_i + \lambda} \leq \frac{\delta}{\delta + \lambda} \rightarrow 0 \quad \text{as } \delta \rightarrow 0. \quad (24)$$

Consequently,

$$\gamma_i \rightarrow 1 \quad \text{as } v_i \rightarrow 0. \quad (25)$$

Thus ASR does not apply a large raw variance-matching correction to channels whose post-pruning activation variance has nearly vanished.

More generally, Eq. (19) implies that each ASR correction is a convex combination of the raw estimate and the identity:

$$\gamma_i \in [\min\{1, \hat{\gamma}_i\}, \max\{1, \hat{\gamma}_i\}]. \quad (26)$$

This property is the stability mechanism used by ASR. It does not make the raw estimator itself bounded, nor does it guarantee that every healthy channel is perfectly repaired. Instead, it ensures that the applied correction is no more extreme than the raw estimate and that the most unreliable low-variance channels are pulled toward no correction.

Degenerate zero-median case. The analysis above assumes $\lambda > 0$. If the median post-pruning variance in a layer is exactly zero, then at least half of the channels have zero or numerically negligible variance on the calibration set. In this degenerate case, the layer contains too little reliable channel-wise information for aggressive multiplicative repair to be well-conditioned. In implementation, this case should be handled conservatively, for example by using a small numerical floor for λ or by falling back toward the identity correction for the affected layer. This behaviour is consistent with the central design principle of ASR: collapsed channels should not be amplified in an attempt to match dense variance.

A.4 Bias Correction and Integration with BatchNorm Recalibration

Pruning can shift activation means as well as variances. After channel-wise rescaling, we optionally adjust the convolutional bias so that the repaired pre-BatchNorm activations match the dense activations at the first moment. Let $\gamma = (\gamma_1, \dots, \gamma_C)^\top$, and denote by $\widehat{\mathbb{E}}[\mathbf{Y}_d]$ and $\widehat{\mathbb{E}}[\mathbf{Y}_p]$ the per-channel sample means over batch and spatial dimensions. If the repaired pre-BatchNorm activations are written as

$$\tilde{\mathbf{Y}}_p = \gamma \odot \mathbf{Y}_p + (\mathbf{b}_{\text{new}} - \mathbf{b}_{\text{old}}),$$

then imposing

$$\widehat{\mathbb{E}}[\tilde{\mathbf{Y}}_p] = \widehat{\mathbb{E}}[\mathbf{Y}_d]$$

gives

$$\mathbf{b}_{\text{new}} = \mathbf{b}_{\text{old}} + \widehat{\mathbb{E}}[\mathbf{Y}_d] - \gamma \odot \widehat{\mathbb{E}}[\mathbf{Y}_p]. \quad (27)$$

For networks with BatchNorm layers, ASR is applied before BatchNorm recalibration. ASR estimates channel-wise repair factors from 64 calibration images using forward evaluation only. BatchNorm recalibration is then performed under the same recalibration budget used for all repair baselines in the corresponding experiment. Thus ASR does not use gradient computation or sparse-model retraining, and it does not change the pruning mask.

B Choice of Calibration Step for Main Reporting

We use calibration step $b=20$ as the primary reporting point for BN Only, LW+BN, and ASR+BN. This choice reflects a practical trade-off. By $b=20$, BatchNorm recalibration has already recovered a substantial portion of its eventual performance across datasets, while the gap between methods remains visible enough to distinguish the effect of post-pruning repair. At smaller calibration budgets, BN statistics are often still too noisy for a stable comparison. At larger budgets, the marginal gains from additional recalibration become smaller and the performance of different repair methods begins to compress toward a common ceiling.

Table 3 and Figure 7 together illustrate this trade-off. Across datasets, step 20 captures most of the recoverable benefit of BN recalibration while remaining early enough to preserve sensitivity to differences among repair methods. For this reason, it provides a stable and informative operating point for the main comparison.

C Robustness Checks and Additional Plots

C.1 Calibration-step trends on CIFAR-100

Figure 8 complements the CIFAR-10 calibration curves in Figure 3 of the main paper by showing top-1 accuracy versus calibration batch size on CIFAR-100. The pattern is broadly consistent with CIFAR-10: ASR+BN shows its clearest advantage over LW+BN in the higher-sparsity settings, especially at 90% sparsity and under NM 2:4 sparsity, while differences among methods narrow as the calibration budget increases.

BN-only accuracy by dataset (median + 95% quantile band)

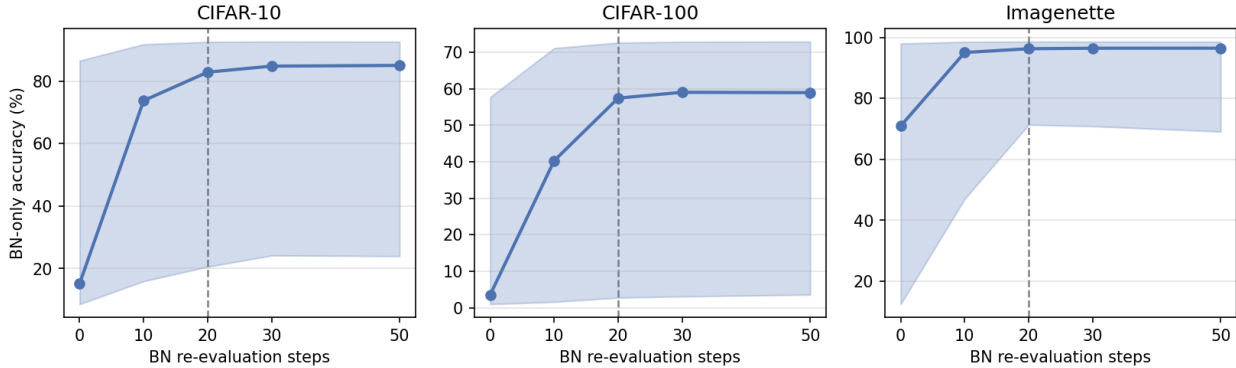


Figure 7: BN Only top-1 accuracy (median and 95% quantile band) as a function of BatchNorm recalibration steps, shown separately for each dataset. The dashed vertical line marks step $b=20$, which captures most of the recoverable gain while retaining useful separation among repair methods.

Table 3: Top-1 accuracy (%) versus BatchNorm recalibration step. Each entry is reported as median [min, max] across evaluated settings. Step 20 is used as the primary reporting point in the main text.

Dataset	Step 0	Step 10	Step 20	Step 30	Step 50
	15.20	73.75	82.86	84.79	85.02
CIFAR-10	[8.60, 86.54]	[15.94, 91.78]	[20.57, 92.53]	[24.17, 92.63]	[23.97, 92.60]
	3.52	40.30	57.47	59.06	58.97
CIFAR-100	[0.96, 57.72]	[1.58, 71.17]	[2.73, 72.67]	[3.07, 72.91]	[3.55, 72.96]
	70.95	95.04	96.28	96.45	96.46
Imagenette	[12.50, 97.98]	[47.03, 98.54]	[71.34, 98.61]	[70.85, 98.60]	[69.10, 98.57]
	23.16	66.01	79.20	80.76	80.74
Overall	[1.00, 97.77]	[2.04, 98.26]	[5.89, 98.33]	[6.46, 98.36]	[7.04, 98.37]

C.2 Pruning Severity and Repair Gap

Figure 9 extend the correlation analysis in Section 5.3 of the main text by reporting results at both $b=10$ and $b=20$, and by including a second severity measure: the layer-wise overshoot $\max(0, \gamma_{LW} - 1)$, which directly quantifies how much layer-wise scaling exceeds the identity on average.

Figure 9 shows the accuracy gap between BN Only and LW+BN as a function of both severity measures. The positive correlation confirms that layer-wise repair degrades relative to BN Only most strongly when pruning induces large variance distortion or large overshoot, consistent with the instability analysis in Section A.3.

Figure 9 shows the corresponding gap between ASR+BN and LW+BN. At $b=20$ (bottom-left panel), the correlation with pruning severity reaches $r=0.61$, $\rho=0.70$, matching the value reported in the main text. At $b=10$ the correlation is weaker ($r=0.19$, $\rho=0.33$), reflecting the additional noise in BN statistics at very small calibration budgets.

C.3 Per-layer Variance Statistics

Figures 10 and 11 show per-layer heatmaps of channel variance statistics for ResNet-18 on CIFAR-100 and VGG-16-BN on CIFAR-10, both at 90% global L1 sparsity. Each row corresponds to one diagnostic statistic (fraction of channels below the 5th percentile of dense variance, 25th and 75th percentile variance ratios, and recovery ratios for LW+BN and ASR+BN), and each column corresponds to one convolutional layer.

For ResNet-18 (Figure 10), the `var_ratio_q75_lw` row shows values well above 1 in the deeper layers (up to 12.6 at `layer3.1.conv1`), indicating systematic over-correction by layer-wise repair. The corresponding `var_ratio_q75_asr` row remains much closer to 1 throughout, confirming that ASR suppresses the overshoot. For VGG-16-BN (Figure 11), over-correction is even more pronounced in the later feature layers (up to 19.4 at `features.40`), which is consistent with the observation in the main text that BN Only outperforms both repair methods on this architecture at 90% sparsity.

C.4 Additional Calibration Curves

Figure 12 extends the structured-sparsity comparison in Table 1 by showing top-1 accuracy versus calibration batch size for ResNet-50 under NM 2:4 structured sparsity across all three datasets. ASR+BN leads BN Only and LW+BN at small calibration budgets on CIFAR-10 and CIFAR-100, with the advantage most visible at $b=10$. On Imagenette, where the fine-tuned dense model is close to ceiling performance, all three methods converge rapidly and the differences are small, consistent with the pattern observed in the main text.

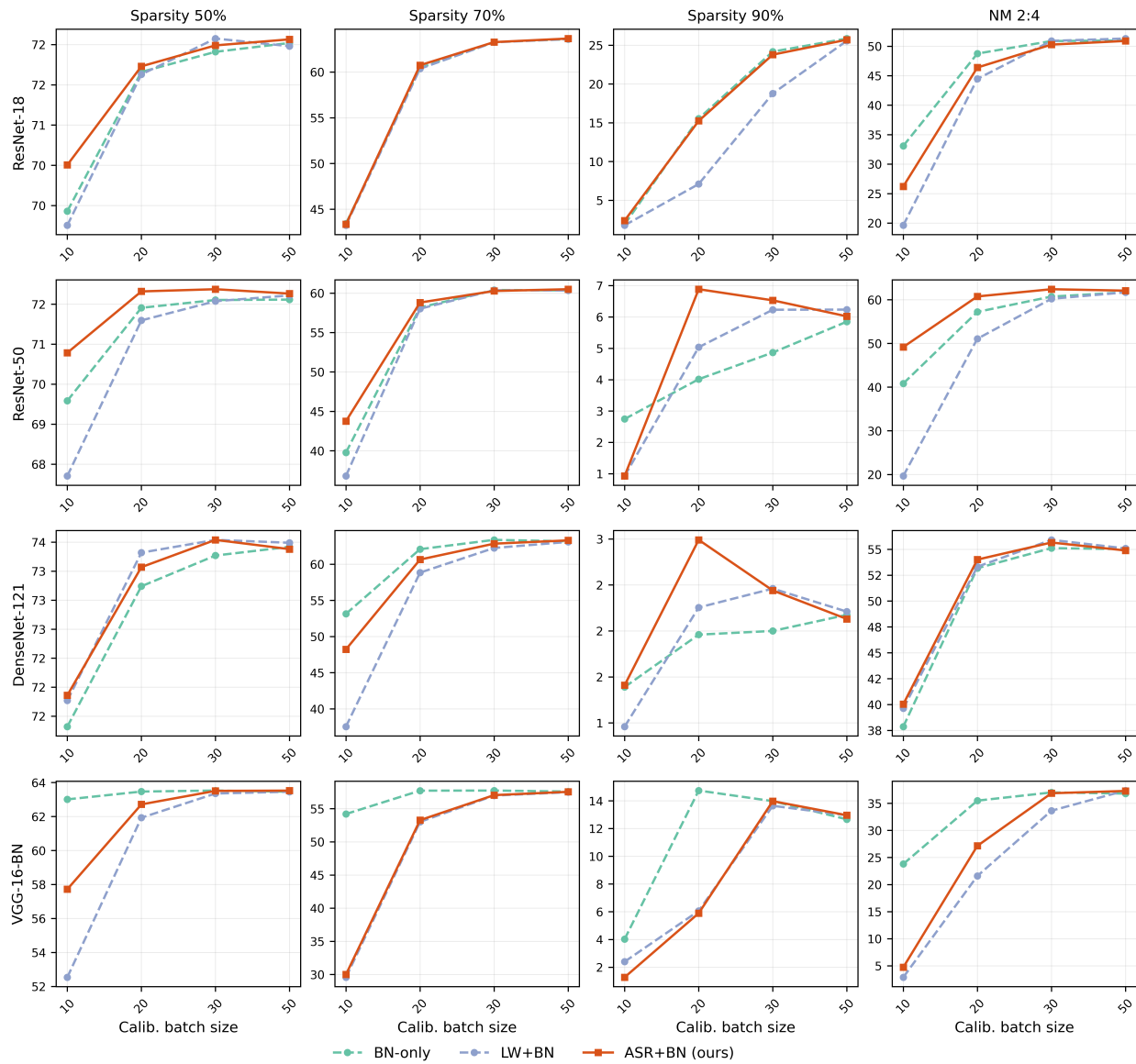


Figure 8: Top-1 accuracy versus calibration batch size on CIFAR-100. The overall trend is consistent with CIFAR-10, with ASR+BN showing the clearest advantage over LW+BN in the higher-sparsity settings.

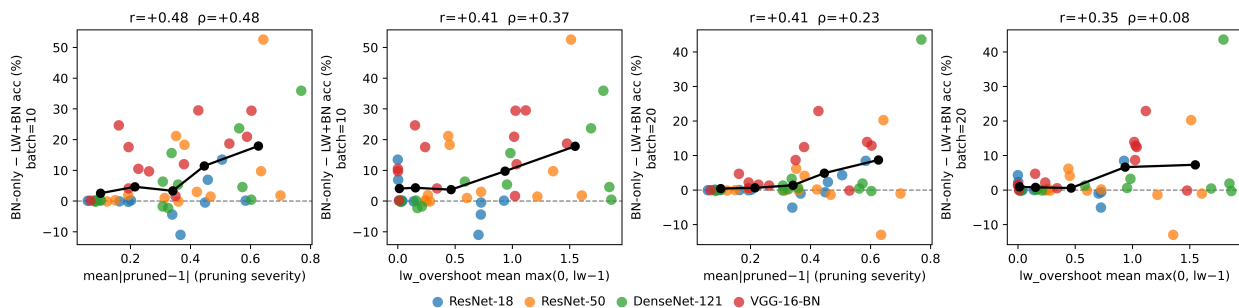


Figure 9: Accuracy gap between BN Only and LW+BN as a function of pruning severity (left column: $\text{mean}|\gamma_{\text{pruned}} - 1|$; right column: layer-wise overshoot $\text{mean}\max(0, \gamma_{LW} - 1)$) at calibration steps $b=10$ (top) and $b=20$ (bottom). Larger severity is associated with a larger advantage for BN Only over layer-wise repair, consistent with the instability identified in Section A.3.

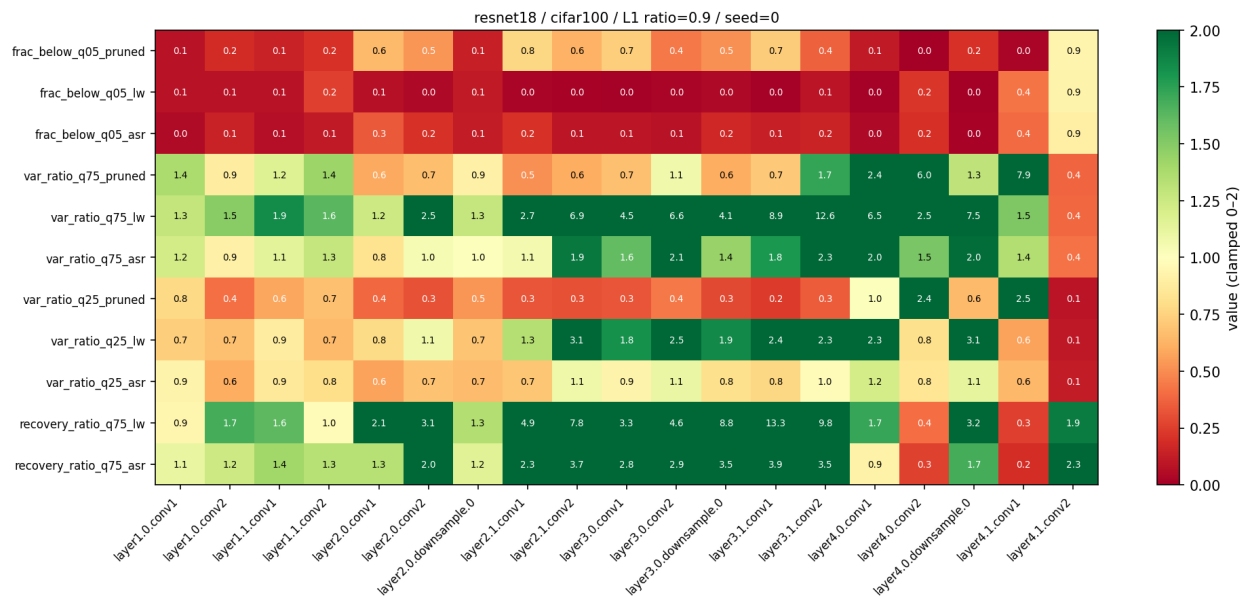


Figure 10: Per-layer channel variance statistics for ResNet-18 on CIFAR-100 at 90% global L1 sparsity. Values clamped to $[0, 2]$. Layer-wise repair over-corrects in the deeper layers (`var_ratio_q75_lw` up to 12.6); ASR remains closer to the dense reference throughout.

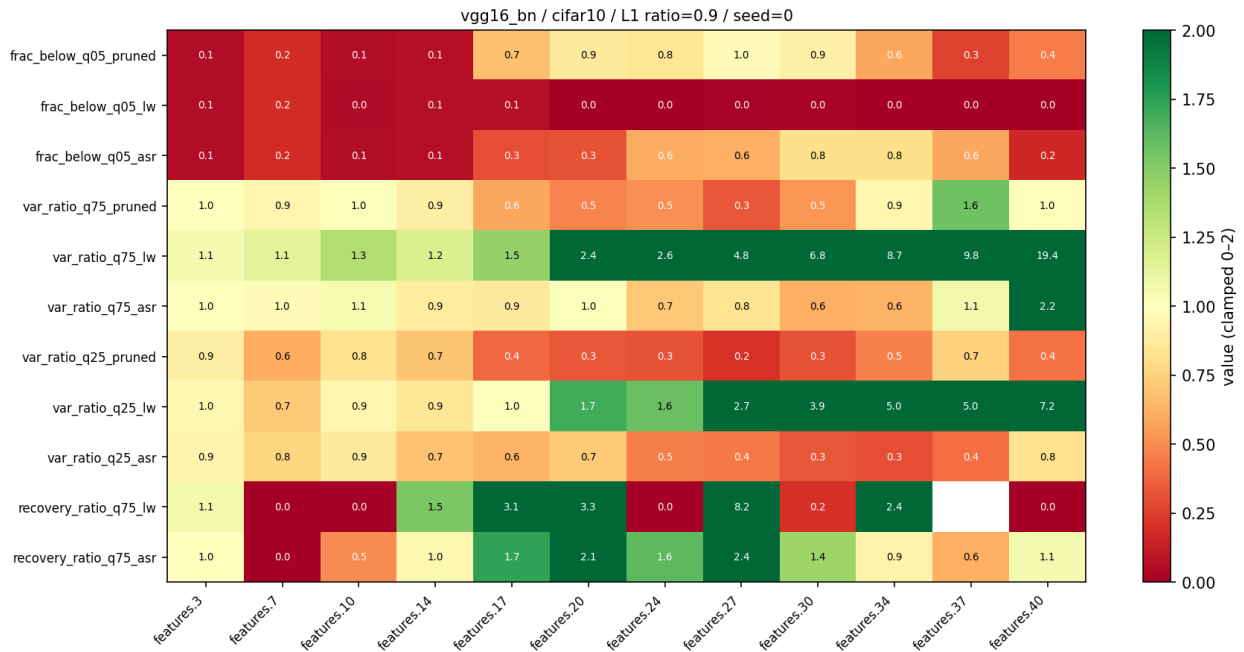


Figure 11: Per-layer channel variance statistics for VGG-16-BN on CIFAR-10 at 90% global L1 sparsity. Over-correction is more severe than in ResNet-18, with `var_ratio_q75_lw` reaching 19.4 at features.40, consistent with BN Only outperforming both repair methods on this architecture.

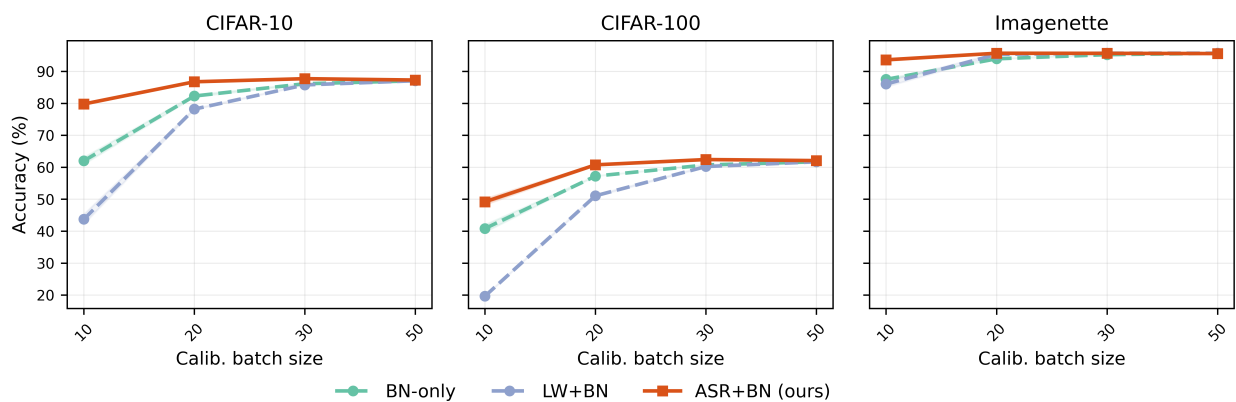


Figure 12: Top-1 accuracy versus calibration batch size for ResNet-50 under NM 2:4 structured sparsity on CIFAR-10, CIFAR-100, and Imagenette. ASR+BN shows the largest advantage at small calibration budgets on the two harder datasets.